

Article

In Vivo Validation of a Cardiovascular Simulation Model in Pigs

Moriz A. Habigt^{1,*}, Jonas Gesenhues², Maike Stemmler², Marc Hein¹, Rolf Rossaint¹
and Mare Mechelinck¹

¹ Anaesthesiology Clinic, Faculty of Medicine, RWTH Aachen University, Pauwelsstr. 30, 52074 Aachen, Germany; mhein@ukaachen.de (M.H.); rossaint@ukaachen.de (R.R.); mmechelinck@ukaachen.de (M.M.)

² Institute of Automatic Control, RWTH Aachen University, Campus-Boulevard 30, 52074 Aachen, Germany; j.gesenhues@irt.rwth-aachen.de (J.G.); m.stemmler@irt.rwth-aachen.de (M.S.)

* Correspondence: mhabigt@ukaachen.de; Tel.: +49-241-80-88179

Abstract: Many computer simulation models of the cardiovascular system, of varying complexity and objectives, have been proposed in physiological science. Every model needs to be parameterized and evaluated individually. We conducted a porcine animal model to parameterize and evaluate a computer simulation model, recently proposed by our group. The results of an animal model, on thirteen healthy pigs, were used to generate consistent parameterization data for the full heart computer simulation model. To evaluate the simulation model, differences between the resulting simulation output and original animal data were analysed. The input parameters of the animal model, used to individualize the computer simulation, showed high interindividual variability (range of coefficient of variation: 10.1–84.5%), which was well-reflected by the resulting haemodynamic output parameters of the simulation (range of coefficient of variation: 12.6–45.7%). The overall bias between the animal and simulation model was low (mean: -3.24% , range: from -26.5 to 20.1%). The simulation model used in this study was able to adapt to the high physiological variability in the animal model. Possible reasons for the remaining differences between the animal and simulation model might be a static measurement error, unconsidered inaccuracies within the model, or unconsidered physiological interactions.

Keywords: computer simulation; cardiovascular system; parameterization; validation; animal model



Citation: Habigt, M.A.; Gesenhues, J.; Stemmler, M.; Hein, M.; Rossaint, R.; Mechelinck, M. In Vivo Validation of a Cardiovascular Simulation Model in Pigs. *Math. Comput. Appl.* **2022**, *27*, 28. <https://doi.org/10.3390/mca27020028>

Received: 25 November 2021

Accepted: 15 March 2022

Published: 18 March 2022

Publisher's Note: MDPI stays neutral with regard to jurisdictional claims in published maps and institutional affiliations.



Copyright: © 2022 by the authors. Licensee MDPI, Basel, Switzerland. This article is an open access article distributed under the terms and conditions of the Creative Commons Attribution (CC BY) license (<https://creativecommons.org/licenses/by/4.0/>).

1. Introduction

Computer simulation models of the cardiovascular system are increasingly used in the development and improvement of ventricular assist devices (VADs) and VAD control algorithms [1–3], as well as in many other fields of cardiovascular research. With an increasing accuracy of the computer simulation models, clinical use is also imaginable but demands the possibility to highly individualize the used models. Examples of possible areas of application are the planning of high-risk operations, such as the correction of congenital heart defects or implantation of biomedical devices (e.g., valves or ventricular assist devices), to predict the cardiovascular reserve of the patient or response to a certain drug therapy. Since the 1960s, when computer simulation of the cardiovascular system started [4,5], many different simulation models have been developed. In addition to the different strategies to implement basic physiological conditions, the various models also differ in complexity and focus on specific physiological phenomena. Generally, three different types of models are distinguishable: myocardial activity can be modelled by a time-varying elastance curve [3,6–12], a sarcomere model [13–15], or isovolumetric contractions [16,17]. In the first case, emphasis is placed on the correct simulation of the starling curve; in the second case, the interaction between sarcomere and ventricular cavity mechanics is addressed; in the third case, the afterload dependency of the heart is stressed.

The arterial system has also been simulated in many ways. Lumped parameter models (“Windkessel models”) [3,18] can be distinguished from tube [14,19–21] and anatomically-based distributed models [22–25]. Another important difference between the described models is the integration of different physiological regulatory mechanisms. Some models focus on the exact simulation of physiological autoregulatory mechanisms, e.g., the baroreceptor reflex [8]. In contrast, other models neglect this mechanism and emphasize further mechanisms, such as left and right ventricular interaction [11,14], coronary blood flow [15], the venous return curve [12], or cardiopulmonary interaction [26].

It is difficult to determine the most accurate and effective way to simulate specific processes in the cardiovascular system. Every simulation model needs to be evaluated individually, has its own advantages and disadvantages, and probably shows different behaviour under different circumstances. Scientists working with these models need to know the differences, possible flaws, and error susceptibility of the models they are working with.

We wanted to assess a full heart computer simulation model, which was previously described by our group [3,27], especially with regard to its ability to be adapted to individual hemodynamic settings. We, therefore, conducted a porcine animal study and used the data as the basis to parameterize the model. Then, we compared the results of the animal study to the simulative results. In a third step, we varied the input parameters to the simulation, in order to determine by which parameters the results were affected the most and must, therefore, be especially critical to time-varying elastance simulation models of the cardiovascular system.

2. Materials and Methods

2.1. Animal Model

2.1.1. Induction and Maintenance of Anaesthesia

All procedures described below are compliant with the Guide for the Care and Use of Laboratory Animals [28] and reviewed and approved by the local animal care committee and governmental animal care office (No. 84-02.04.2013. A476 and 8.87-50.10.45.08.257; Landesamt für Natur, Umwelt und Verbraucherschutz Nordrhein-Westfalen, Recklinghausen, Germany). Thirteen healthy pigs (*German landrace*, 46.26 kg \pm 4.46 kg bodyweight [BW]) received premedication by intramuscular injection of 4 mg/kg azaperone (Elanco Tiergesundheit AG, Basel, Switzerland) and were anaesthetized by intravenous injection of 3 mg/kg BW propofol (Hexal AG, Holzkirchen, Germany) for oral intubation. Anaesthesia was maintained by the insufflation of 0.9–1.2 vol% isoflurane and continuous application of 6–8 μ g/kg BW/h fentanyl (Ratiopharm GmbH, Ulm, Germany). Normoventilation was achieved by the application of a tidal volume of 8–10 mL/kg BW and monitored by expiratory CO₂ measurement (PaCO₂ 36–42 mmHg) and regular arterial blood gas analysis. Electrolytes and blood glucose were similarly monitored by arterial blood gas analysis and held in a physiological range. The haematocrit was stabilized by the infusion of 6–10 mL/kg BW/h of a balanced crystalloid solution (Sterofundin Iso Braun, B.Braun AG, Melsungen, Germany) solution and application of 500 mL of a balanced colloid solution (Gelafundin Iso Braun) after instrumentation. The body temperature was held constant (38 °C) by the use of an airflow warming blanket.

2.1.2. Surgical Instrumentation

After dissecting the neck vessels on the right side, one central venous catheter was introduced into the right internal jugular vein, and two 12 F sheaths were introduced into the right carotid artery. A median thoracotomy was performed, and the pericardium was opened longitudinally. The aorta and pulmonary arteries were separated, and a perivascular ultrasound transit time flow probe (MA 20 PAX; Transonic Systems Europa, Maastricht, The Netherlands) was positioned centrally around each vessel and connected to a flow meter (T402-PV, Transonic Systems Europa). To measure pulmonary and aortic pressure, a solid-state pressure sensor (CA-61000-PL, CD Leycom, Zoetemeer, The Netherlands)

was introduced through a stab wound in the right ventricular outflow tract, with another equal sensor through the sheath in the right carotid artery. The pressure sensors were positioned 3–4 cm distal to the respective valves (i.e., the pulmonary and aortic valves) and connected to a pressure interface (Sentron, CD Leycom). A multi-segment dual-field 7F conductance catheter (SPR-570-7; Millar Instruments, Houston, TX, USA) was placed through the apex of the right ventricle along the outflow track. A second equal catheter was introduced through the second right carotid sheath and aortic valve, with the tip placed in the left ventricular apex. Echocardiographic imaging was performed to verify the correct positioning of the catheter. The volume segments of the catheters were connected to two signal processors (Sigma-5 DF, CD Leycom). To avoid electrical interferences and for simultaneous biventricular measurements, the excitation frequency of one processor was modified from 20 to 15 kHz. The pressure sensors of the catheters were connected to a pressure interface (PCU-2000; Millar Instruments). Through a sheath in the right femoral vein, a 7F balloon catheter was placed in the inferior vena cava, in order to perform a short-term preload reduction during apnoea and constant positive end expiratory pressure (PEEP). A schematic of the instrumentation is shown in Figure 1. After the completion of instrumentation, the animals recovered for 30 min, with continued isoflurane and fentanyl narcosis, in order to achieve stable blood pressure, cardiac output (CO), and normothermia.

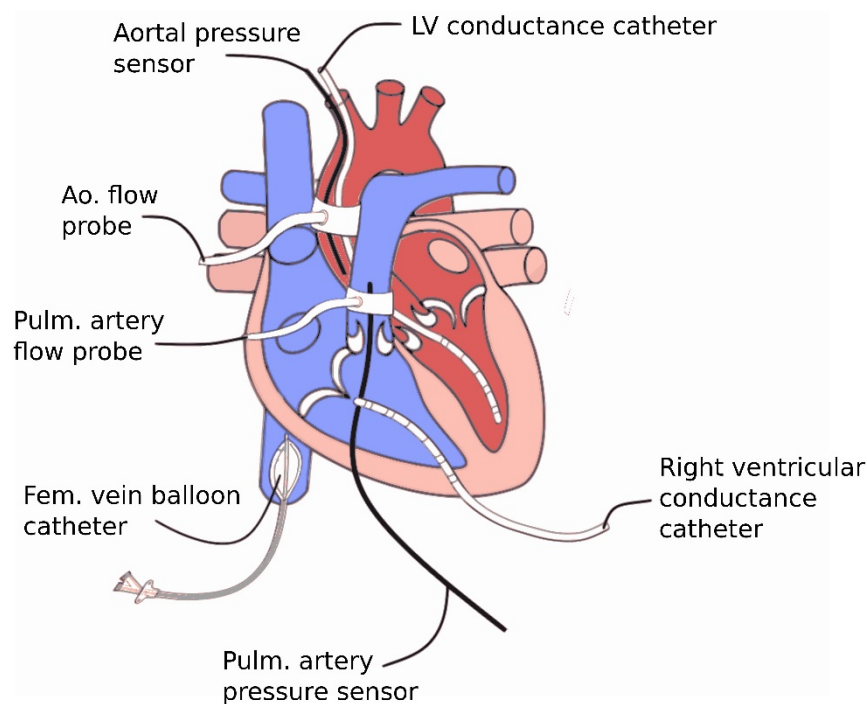


Figure 1. Instrumentation of the heart with left ventricular conductance catheter, aortal pressure sensor, aortal flow probe, pulmonary artery flow probe, femoral vein balloon catheter, pulmonary artery pressure sensor, and right ventricular conductance catheter. Figure is a modification of figure “Heart normal” by Eric Pierce [29]. The original figure can freely be published under CC BY-SA license (<https://en.wikipedia.org/wiki/User:Wapcaplet>, accessed on 16 March 2022).

2.2. Data Acquisition and Calculations

Signals were acquired continuously, at a sampling rate of 1000 Hz, using a data acquisition device (Powerlab, AD Instruments, Dunedin, New Zealand) and software (LabChart, AD Instruments).

The conductance volume values were calibrated prior to the measurement of each animal. Therefore, the volume signal was corrected by stroke volume (SV), obtained from the aortic flow probe (slope factor α) and parallel conductance, calculated from venous hypertonic saline injections, as described previously [30–32]. The signals were finally

analysed off-line with custom-made software (CIRCLAB 2020; Paul Steendijk, Leiden, The Netherlands).

Global haemodynamics were described by heart rate (HR), mean arterial pressure (MAP), CO, SV, and ejection fraction (EF). End-systolic pressure (P_{ES}), volume (V_{ES}), end-diastolic pressure (P_{ED}), and volume (V_{ED}) were used to describe the ventricular dimensions. These parameters were calculated as averages over 20 s. Systolic function was characterized by the end-systolic pressure volume relationship (ESPVR) and preload recruitable stroke work (PRSW), obtained from pressure-volume loops acquired during short preload reduction by caval occlusion during apnoea. The ESPVR is the linear regression of the end-systolic pressure volume points and characterized by the slope, end-systolic elastance (E_{ES}), and x-axis intercept (V_{0_ES}). The PRSW is the slope of the linear regression between the ventricular stroke work (SW) and end-diastolic volume (EDV). The passive (stiffness) components of ventricular relaxation were displayed by the exponential regression of the end-diastolic pressure volume points (end-diastolic pressure volume relationship: EDPVR), which was characterized by the indices P_0 , V_0 , and λ .

$$P_{ED} = P_{0_ES} * (\exp(\lambda(V_{ED} - V_0)) - 1) \tag{1}$$

as described by Wang et al. [32]. We iteratively calculated the single indices of the equation. Values from three to five consecutive recordings were averaged.

The compliant characteristics (Cs) of the Windkessel vessels were calculated by dividing the SV by the difference in systolic and diastolic pressure (pulse pressure [PP]), as previously described [33]. Fourier series expressions for pressure and flow signals of 20 s duration were used to calculate systemic vascular resistance and impedance. The impedance modulus at each frequency was calculated as the ratio between pressure and flow moduli (amplitudes). The total resistance (Z_0) and characteristic impedance (Z_c) were derived from moduli at zero frequency and an average of moduli between 2 and 15 Hz [34].

2.3. Simulation Model

An electrical analogue of the circulation model is given in Figure 2.

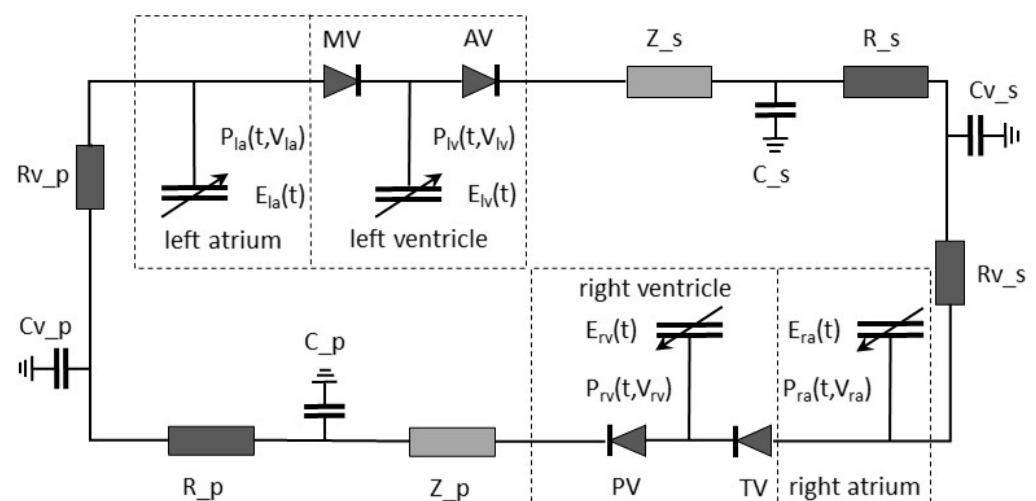


Figure 2. Electrical analogue of the circulation model. The single components are denoted by the following designation. Vascular and specific resistance: R, Z. Vascular compliances: C. Venous system: v. systemic circulatory system: _s. Pulmonary circulatory system: _p. Valves: TV, PV, MV, and AV. Elastance function of the atria and ventricles: E. A closer description of the single components is given in Table S1 in the supplemental materials.

A three-element Windkessel model was used to describe the systemic and pulmonary vascular systems. Each arterial system consisted of two hydraulic resistances with

$$Q_{Resistance}(t) = \frac{\Delta P_{Resistance}(t)}{R_i} \tag{2}$$

and an interconnected compliancy with

$$P_{Compliancy}(t) = \frac{V_{Compliancy}(t)}{C_i} \tag{3}$$

The venous system consisted of one hydraulic resistance and one connected compli-ance only.

The pulsation of the heart chambers and atria was modelled as a nonlinear time-varying elastance, where the ventricle volume determined the corresponding time-varying pressures $P(t) = f(V(t) - V_0)$, with unstressed volumes V_0 . The time varying-elastance function used in our model was based on the work of Chung et al. [35], whereas concrete values were obtained from previously published animal data [36]. The filling and ejection phases were characterized by the exponential EDPVR

$$P_{ED}(V) = P_{0_ES}^{\lambda(V-V_{0_ED})} - 1 \tag{4}$$

and linear ESPVR

$$P_{ES}(V) = E_{ES} \cdot V + V_{0_ES} \tag{5}$$

where E_{ES} is the slope, and V_{0_ES} is the x-axis offset of the specific relationship.

On this basis, the instantaneous pressure could be determined by

$$P(V, t) = \varphi(t) \cdot P_{ES}(V) + (1 - \varphi(t)) \cdot P_{ED}(V). \tag{6}$$

The activation function, $\varphi(t)$, triggered the systole and ran periodically between 0 and 1. One period of the activation function was defined as the sum of exponential functions

$$\Phi(t) = \sum_{i=1}^5 A_i \cdot e^{-\left(\frac{t-B_i}{C_i}\right)^2} \tag{7}$$

The parameters A_i , B_i , and C_i were obtained using experimental data, as described by Gesenhues et al. [17]. This function was used with a normalized time signal

$$t_N = (t - k_D) \cdot HR/60 - \text{floor}((t - k_D) \cdot HR/60) + k_O \tag{8}$$

to obtain the activation function signal $\varphi(t)$

$$\varphi(t) = \Phi(t = t_N(t)). \tag{9}$$

The normalized time signal, t_N , restarts after each beat was implemented, using a shifted sawtooth wave with a frequency equal to the heart rate. The floor function mapped a real number to the largest previous integer. The shape of the activation function and consecutive left ventricular volume and pressure values for animal 4 are shown in Figure 3.

$$Q_{Valve,ideal}(t) = \begin{cases} \frac{\Delta P_{Valve}(t)}{R_{Valve}} & \text{if } \Delta P_{Valve}(t) > 0 \\ 0 & \text{if } \Delta P_{Valve}(t) \leq 0 \end{cases} \tag{10}$$

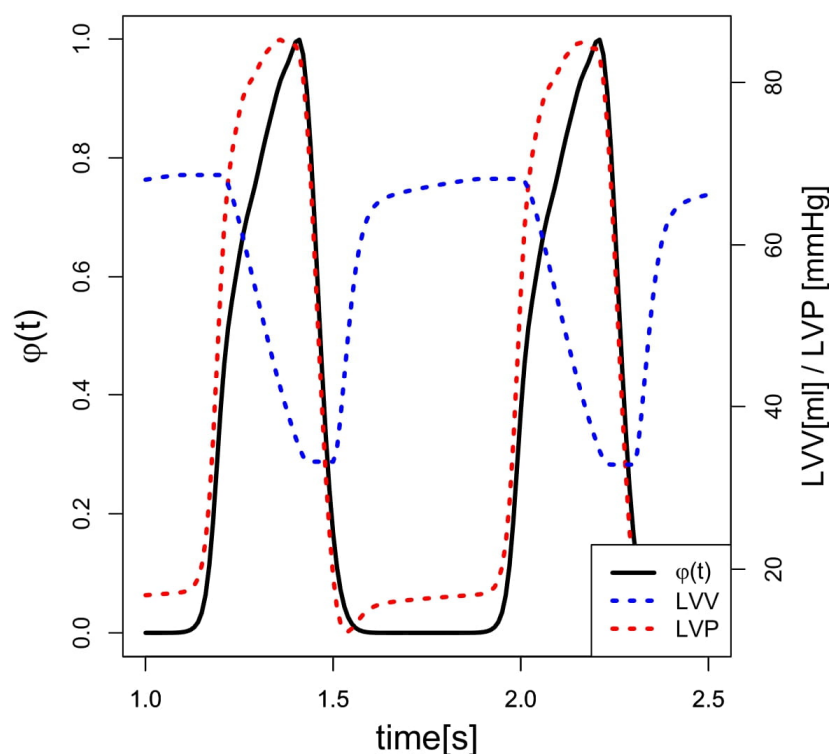


Figure 3. Activation function. Simulated activation function ($\phi(t)$ —black), consecutive left ventricular volume (LVV—blue), and left ventricular pressure (LVP—red) in animal 4.

The heart valves acted as non-return valves, which meant that they allowed flow at a given hydraulic resistance R_{Valve} in only one direction, depending on the pressure differential ΔP_{Valve} across the valve. A detailed description of the single components is given in Table S1 of the supplemental materials.

This simplified closed circuit model of the whole circulatory system was implemented in the open (object-oriented) modelling language Modelica[®]. We ran this model in our self-developed simulation tool ModeliChart, which was especially designed for clinical users and allows for independently performing in silico studies in real time [37]. The model was a full circulatory model, as previously described [3,27]. In contrast to our latter study [3], we did not use a VAD in this study.

To parametrize the simulation according to the animal data, we used the general configuration of settings described in [3], which is based on the data described in the literature, and only individually adjusted ten input parameters. HR, E_ES, V0_ES, P0_ED, V0_ED, λ , C, Z0, and Zc were calculated, as described above, and could be directly adopted into the simulation. Each animal was simulated individually. The unstressed volume of the systemic venous compliance (V0_sC) was used to adjust the ventricular preload until the EDV between the simulation and animal matched. A short increase of V0_sC was used as a virtual preload reduction to calculate the slope of the PRSW, as shown in Figure 4. The respective values of P_ES, P_ED, V_ES, V_ED, SV, EF, SW, MAP, and PRSW were used to compare individual values from animals and simulation.

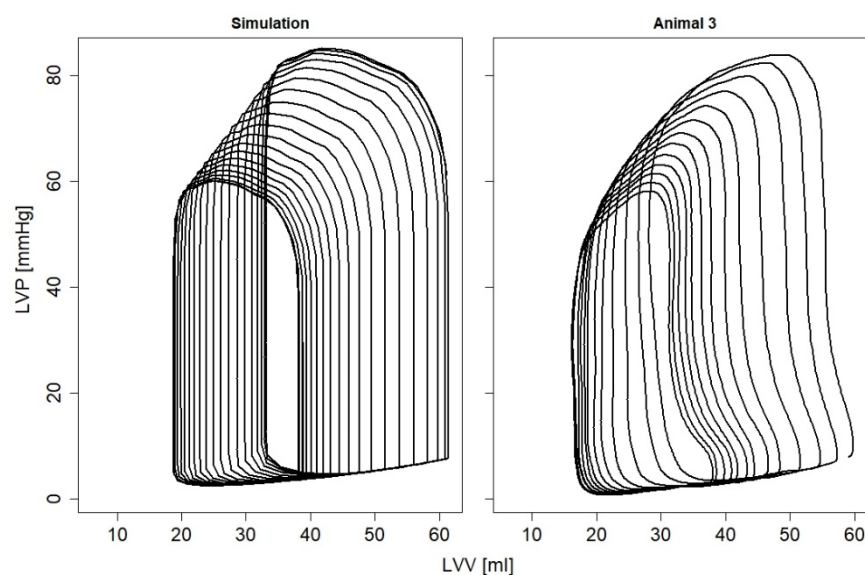


Figure 4. Pressure and volume data of a virtual and in-vivo preload reduction of the simulated and real animal 3. LVP: left ventricular pressure; LVV: left ventricular volume.

2.4. Statistics

The results are displayed as the mean and standard deviation (SD) (PRISM 6.0, GraphPad Software, San Diego, CA, USA). The coefficient of variation (CV) was used to describe interindividual variability and Bland–Altman plots to describe the agreement (bias) and its 95% limits (PRISM 6.0, GraphPad Software).

3. Results

Three out of thirteen pigs could not be analysed: two pigs showed acute bleeding during dissection and the other pig showed an atrial septal defect, which only came obvious during the operation. The input parameters, which were necessary to individualize the simulation model, demonstrated a large interindividual variability (CV = 10.1–84.5%) for the systolic and diastolic function parameters of the left ventricle and parameters characterizing the systemic circulation (Table 1).

The resulting haemodynamic output parameters from the simulation (Figure 4) similarly showed a high interindividual variation (CV = 12.6–45.7%) and low overall bias between the two datasets could be observed (mean: −3.24%; range: −26.5% to 20.1%). The smallest bias between the animal model and simulation was reached for the EF and MAP, with each 5% mean difference between all values. The largest bias, with a mean difference of 27–28% between all values, was observed in the P_{ED} and PRSW (Table 2).

The best matches between the animal model and simulation (under 5% difference of the values) were reached for SV in animals 9 and 10, in the V_{ES} in animals 2, 5, and 10, in the EF in animals 9 and 10, in the MAP in animals 3, 5, 7, 9, and 10, and in the PRSW in animal 1. The most pronounced differences between animal study and simulation (more than 25% difference) were observed in the P_{ED} in animals 2, 8 and 10, the SW in animals 2, 7, 8, and 10, and the PRSW in animals 2, 3, 4, 7, 8, and 10 (Figure 5).

Table 1. Parameters derived from the animal studies, which were used to parametrize the simulation model: HR: heartrate [bpm], E_ES: slope of the ESPVR [mmHg/mL], V0_ES: unstressed volume of the ESPVR [mL], λ : coefficient of the exponential EDPVR, P0_ED: coefficient of the exponential EDPVR [mmHg], V0_ED: unstressed volume of the EDPVR [mL], Cs: systemic arterial compliance [mmHg/mL], Z0: systemic arterial resistance [mmHg*s/mL], Zc: specific aortal resistance [mmHg*s/mL], V0_sC: unstressed volume of the systemic venous compliance [mL], and CV: coefficient of variation [%].

Input Parameter	Animal	HR	E_ES	V0_ES	λ	P0_ED	V0_ED	Cs	Z0	Zc	V0_sC (Simulation Only)
Simulation/Animal	1	101	1.33	-19.02	0.0365	0.2126	-19.36	1.7298	0.7341	0.0894	1100
	2	91	1.14	-28.94	0.0478	0.0394	-50.48	0.9835	1.0017	0.1029	1865
	3	100	1.41	-23.62	0.0263	0.3675	-63.38	1.7140	1.0959	0.1102	1700
	4	75	1.01	-48.25	0.0253	0.7728	-55.30	1.5443	1.3407	0.0944	1680
	5	79	1.13	-51.44	0.0236	0.2142	-64.57	2.2253	1.2959	0.0994	1382
	6	84	1.60	-8.09	0.0254	0.3502	-67.20	1.9238	0.8044	0.0888	580
	7	85	0.80	-48.74	0.0280	0.5369	-38.80	1.7860	0.7217	0.0840	1060
	8	91	1.04	-30.67	0.0444	0.0110	-80.21	1.7580	0.8584	0.1142	1600
	9	98	1.52	-24.77	0.0218	0.5375	-61.07	1.4927	1.1763	0.1074	1730
	10	106	1.34	-14.98	0.0413	0.0053	-113.60	1.2890	0.7172	0.0951	1250
Mean	49.2	1.23	-29.85	0.0320	0.3047	-61.4	1.6446	0.9746	0.0986	1395	
CV [%]	22.0	20.28	50.4	29.8	84.5	40.5	20.8	24.8	10.1	28.6	

Table 2. Results of the Bland–Altman analysis. Shown are the mean of the difference between in vivo data and simulation in percentage (BIAS [%]), 95% limits of agreement, and coefficient of variation for the end-systolic and -diastolic pressure (P_ES, P_ED), stroke volume (SV), end-diastolic and -systolic volume (V_ED, V_ES), ejection fraction (EF), stroke work (SW), mean arterial pressure (MAP), and preload recruitable stroke work (PRSW).

	P_ES	P_ED	SV	V_ED	V_ES	EF	SW	MAP	PRSW
BIAS [%]	13.1	28.0	-21.6	-0.1	9.8	-4.9	-21.3	-5.0	-27.2
95% Limits of Agreement									
From	-3.6	-8.9	-35.4	-1.7	-13.6	-27.4	-49.7	-19.0	-79.5
To	29.9	64.8	-7.7	1.5	33.3	17.6	7.0	8.9	25.1
Coefficient of variation	15.4	45.7	22.7	20.2	24.9	12.6	29.1	17.1	18.0

In animal 2, the percentage difference between the animal model and simulation for P_ED, P_ES, and SW did not lie within an agreement interval of two standard deviations. Similar results were obtained for the PRSW in animal 7 (Figure 6).

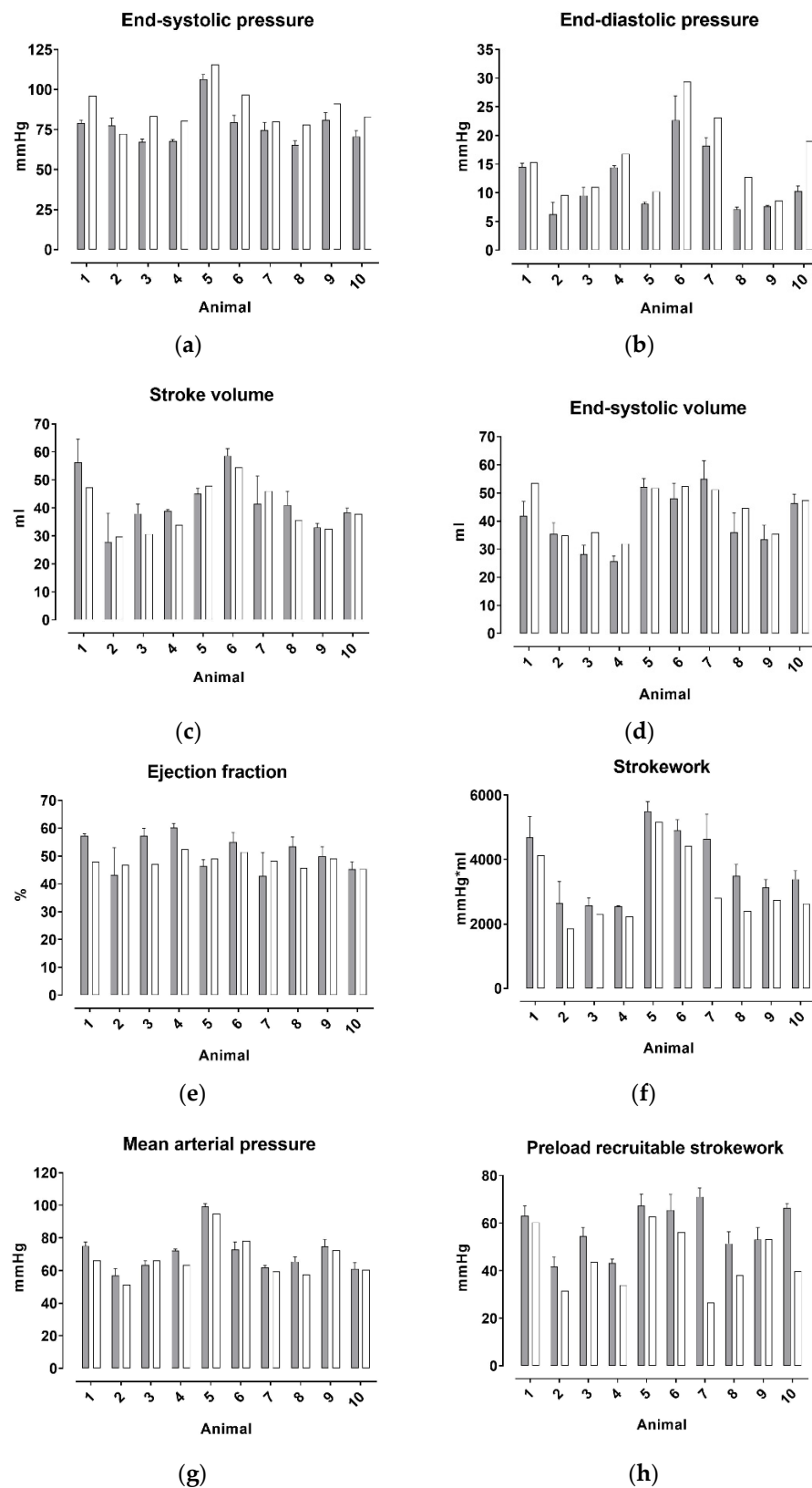


Figure 5. Comparison of animals and simulation. Comparison between the results for the output parameters of animal study (grey) and computer simulation (white) (mean \pm SD) of selected haemodynamic parameters: end-systolic pressure (a), end-diastolic pressure (b), stroke volume (c), end-systolic volume (d), ejection fraction (e), stroke work (f), mean arterial pressure (g) and preload recruitable stroke work (h).

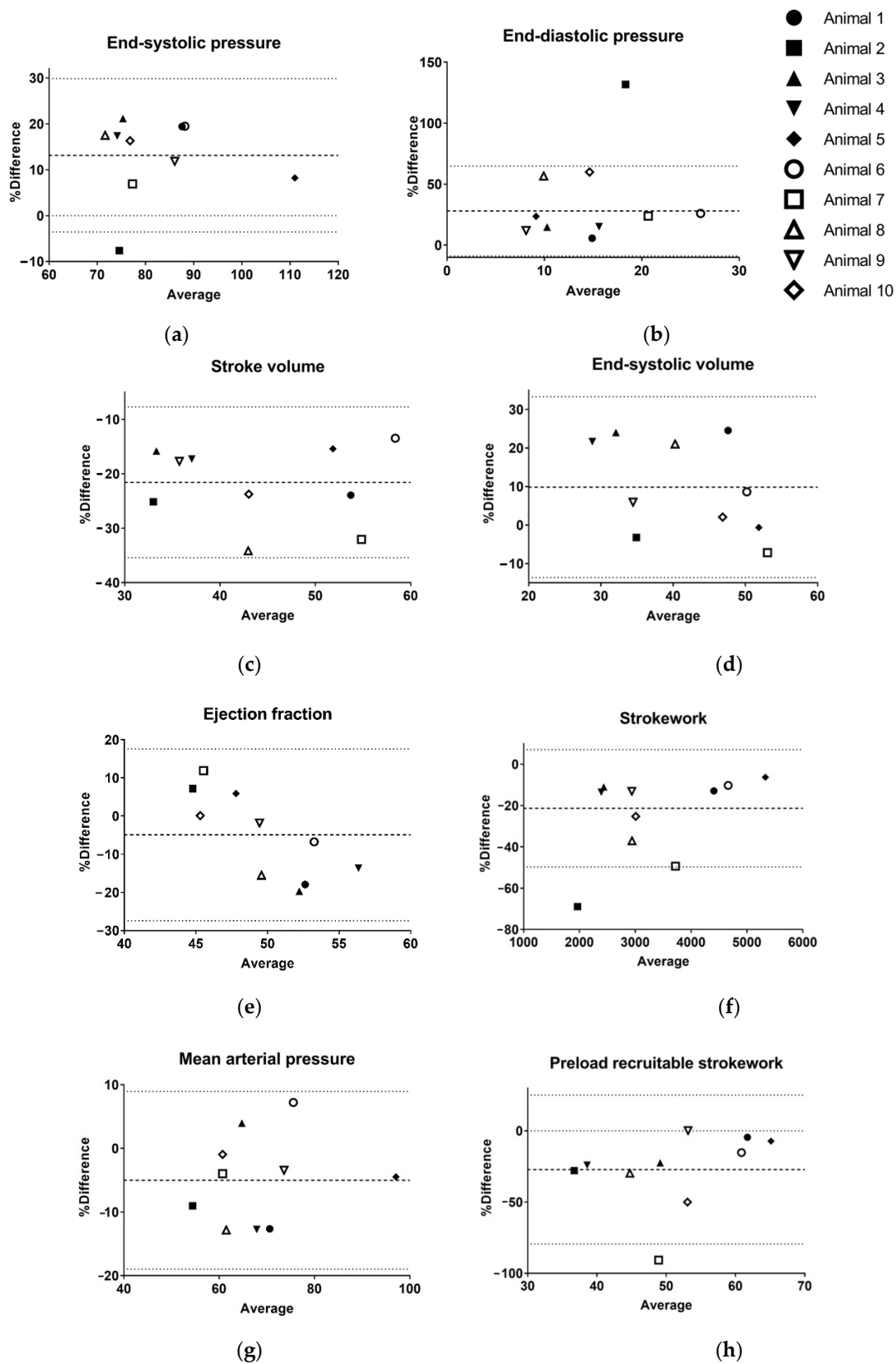


Figure 6. Bland–Altman plots for output parameters of selected haemodynamic parameters: end-systolic pressure (a), end-diastolic pressure (b), stroke volume (c), end-systolic volume (d), ejection fraction (e), stroke work (f), mean arterial pressure (g) and preload recruitable stroke work (h). The mean difference between the in vivo and simulation data, in percentage, is shown as a detached line. The 95% limits of agreement are indicated by dotted lines.

4. Discussion

Our data show a high interindividual variability of parameters, characterizing cardiac function and systemic circulation, among the single animals, and good agreement between simulation and in vivo data. This high interindividual variability is also present in the simulative results, which suggests that a relatively simple computer simulation, in the form of our approach (time varying elastance, linear ESPVR, exponential EDPVR, and three-element Windkessel model), can adapt to a high physiological variability.

The observed differences between simulation and animal might be a static measurement failure, which might result from unknown inaccuracies within the model (e.g., determination of systemic compliance) or unconsidered physiological interactions. There are two conditions that make our simulation prone to static measurement failure. First, minimal changes in the exponential EDPVR have a substantial impact on the simulation results; second, the parameterization of the three-element Windkessel model has inherent problems in determining the compliance and resulting characteristic impedance.

The problem of determining systemic compliance has been an ongoing issue for several decades. Several methods have been proposed and discussed in earlier publications [33,38–40]. We decided to apply the stroke volume-to-pulse pressure ratio method [38], for reasons of substantive conviction and practicability. How this choice influences the accuracy of our simulation model is difficult to estimate. Comparing an application of the different methods within our simulation model lies beyond the scope of this paper.

Considering the Bland–Altman plot of the simulated EF (Figure 6), the distribution of the observed differences between the animal and simulation models implies a linearity that might be evidence for a systematic error: in the case of a high EF in the animal, the EF in the simulation is systematically underrated and vice versa.

We decided to implement the ESPVR as the linear ratio of pressure and EDV. Considering the literature, it is not clarified whether this strategy is correct. Some authors describe the ESPVR as linear [41–43], while others describe it as parabolic [44–46].

In our model, the contractility of the ventricle is simulated by a time-varying elastance function. It could be discussed whether this strategy is the best approach. Modelling the time-varying elastance as being load-independent might not apply, at least when the cardiac load is changed by a VAD [47]. Due to a lack of other direct comparisons between animal and simulated data, it is not clear whether other approaches to model cardiac activity [13–16] are superior to our approach.

As mentioned above, there are also unconsidered physiological mechanisms not included in this model, which might be underestimated in their importance. In the current simulation model, we do not consider the ventricular interaction through the ventricular septum, as it has been done by other groups [11,14,48]. Simulating the interventricular septum as a rigid ventricular wall might insufficiently mirror phenomena in certain situations, e.g., when the simulation model is used to simulate integrated VAD pumps at a high pump speed, where suction effects might occur. Additionally, we did not model the interaction between the coronary perfusion and contractility of the ventricles [15], cardiopulmonary pressure interaction [26], or venous return curve [12]. Autoregulation mechanisms, such as the baroreceptor reflex [8] or Anrep effect [49], are also neglected. The disregard of these mechanisms might seem careless but offers the advantage of a relatively simple computer model, which seems favourable, regarding teaching purposes and clinical implementation. Moreover, the simplicity of the simulation model enables the augmentation of the model by certain features, according to the respective scientific question. For example, the interventricular wall interaction presented in the model of Smith et al. [11] could also be introduced in our model, as both models are based on the time varying elastance.

Another factor that has a high impact on the simulatory results is the modelling of the vascular system. We chose the three-element Windkessel model [50], as this model has been well-examined and established [9,12,13]. However, there are other approaches [14] that might be favourable, considering certain problems, e.g., the difficult determination of compliance and resulting characteristic impedance, as mentioned above.

Our animal data vary significantly between the different healthy animals. If human data show comparable variability, which can be assumed, especially in ill patients, then simulation algorithms for clinical decision-making must be easily adaptable and simple to parametrize, which will be easily achievable with simple models.

5. Conclusions

The direct clinical use of our model does yet not seem feasible, as the parameterization values must be generated invasively. However, the presented data and approaches might help to develop simple, reliable computer simulation models that might be transferred to the clinic in the future.

Thus, the simulation of cardiovascular processes is a reliable tool, if existing limitations are considered. To further improve the accuracy of cardiovascular computer simulation models and transfer these tools to the clinic, further studies are needed.

Supplementary Materials: The following supporting information can be downloaded at: <https://www.mdpi.com/article/10.3390/mca27020028/s1>, Table S1: Non-individualized simulation parameters.

Author Contributions: Conceptualization, M.A.H., M.H. and M.M.; software, J.G. and M.A.H.; investigation, M.A.H., J.G., M.S., M.H. and M.M.; formal analysis, M.A.H. and M.H.; data curation, M.A.H. and M.H.; writing—original draft preparation, M.A.H.; writing—review and editing, M.H. and M.M.; visualization, M.A.H.; funding acquisition, R.R. All authors have read and agreed to the published version of the manuscript.

Funding: This research was funded by the German Research Foundation (DFG), as project Smart Life Support 2.0, grant number 65/15-1 RO 2000/17-1.

Institutional Review Board Statement: All procedures described in this study are compliant with the Guide for the Care and Use of Laboratory Animals and reviewed and approved by the local animal care committee and governmental animal care office (No. 84-02.04.2013. A476 and 8.87-50.10.45.08.257; Landesamt für Natur, Umwelt und Verbraucherschutz Nordrhein-Westfalen, Recklinghausen, Germany).

Data Availability Statement: The datasets generated and analyzed during the current study are available from the corresponding author on reasonable request.

Conflicts of Interest: The authors declare no conflict of interest.

References

1. Scardulla, F.; Pasta, S.; D'Acquisto, L.; Sciacca, S.; Agnese, V.; Vergara, C.; Quarteroni, A.; Clemenza, F.; Bellavia, D.; Pilato, M. Shear stress alterations in the celiac trunk of patients with a continuous-flow left ventricular assist device as shown by in-silico and in-vitro flow analyses. *J. Heart Lung Transplant.* **2017**, *36*, 906–913. [[CrossRef](#)] [[PubMed](#)]
2. Scardulla, F.; Bellavia, D.; D'Acquisto, L.; Raffa, G.M.; Pasta, S. Particle image velocimetry study of the celiac trunk hemodynamic induced by continuous-flow left ventricular assist device. *Med. Eng. Phys.* **2017**, *47*, 47–54. [[CrossRef](#)]
3. Habigt, M.; Ketelhut, M.; Gesenhues, J.; Schrodel, F.; Hein, M.; Mechelinck, M.; Schmitz-Rode, T.; Abel, D.; Rossaint, R. Comparison of novel physiological load-adaptive control strategies for ventricular assist devices. *Biomed. Tech. Berl.* **2017**, *62*, 149–160. [[CrossRef](#)] [[PubMed](#)]
4. Noordergraaf, A.; Verdouw, P.D.; Boom, H.B. The use of an analog computer in a circulation model. *Prog. Cardiovasc. Dis.* **1963**, *5*, 419–439. [[CrossRef](#)]
5. Guyton, A.C.; Coleman, T.G.; Granger, H.J. Circulation: Overall regulation. *Annu. Rev. Physiol.* **1972**, *34*, 13–44. [[CrossRef](#)] [[PubMed](#)]
6. Suga, H.; Sagawa, K.; Shoukas, A.A. Load independence of the instantaneous pressure-volume ratio of the canine left ventricle and effects of epinephrine and heart rate on the ratio. *Circ. Res.* **1973**, *32*, 314–322. [[CrossRef](#)]
7. Leaning, M.; Pullen, H.E.; Carson, E.R.; Finkelstein, L. Modelling a complex biological system: The human cardiovascular system—1. Methodology and model description. *Trans. Inst. Meas. Control.* **1983**, *5*, 71–86. [[CrossRef](#)]
8. Ursino, M. Interaction between carotid baroregulation and the pulsating heart: A mathematical model. *Am. J. Physiol.* **1998**, *275*, H1733–H1747. [[CrossRef](#)]
9. Segers, P.; Stergiopoulos, N.; Schreuder, J.J.; Westerhof, B.E.; Westerhof, N. Left ventricular wall stress normalization in chronic pressure-overloaded heart: A mathematical model study. *Am. J. Physiol. Heart Circ. Physiol.* **2000**, *279*, H1120–H1127. [[CrossRef](#)]
10. Vollkron, M.; Schima, H.; Huber, L.; Wieselthaler, G. Interaction of the Cardiovascular System with an Implanted Rotary Assist Device: Simulation Study with a Refined Computer Model. *Artif. Organs* **2002**, *26*, 349–359. [[CrossRef](#)]

11. Smith, B.W.; Chase, J.G.; Nokes, R.I.; Shaw, G.M.; Wake, G. Minimal haemodynamic system model including ventricular interaction and valve dynamics. *Med. Eng. Phys.* **2004**, *26*, 131–139. [[CrossRef](#)] [[PubMed](#)]
12. Colacino, F.M.; Moscato, F.; Piedimonte, F.; Arabia, M.; Danieli, G.A. Left ventricle load impedance control by apical VAD can help heart recovery and patient perfusion: A numerical study. *ASAIO J.* **2007**, *53*, 263–277. [[CrossRef](#)] [[PubMed](#)]
13. Welp, C.; Werner, J.; Böhringer, D.; Hexamer, M. Investigation of cardiac and cardio-therapeutical phenomena using a pulsatile circulatory model. *Biomed. Tech.* **2004**, *49*, 327–331. [[CrossRef](#)]
14. Arts, T.; Delhaas, T.; Bovendeerd, P.; Verbeek, X.; Prinzen, F.W. Adaptation to mechanical load determines shape and properties of heart and circulation: The CircAdapt model. *Am. J. Physiol. Heart Circ. Physiol.* **2005**, *288*, H1943–H1954. [[CrossRef](#)]
15. Bovendeerd, P.H.; Borsje, P.; Arts, T.; van De Vosse, F.N. Dependence of intramyocardial pressure and coronary flow on ventricular loading and contractility: A model study. *Ann. Biomed. Eng.* **2006**, *34*, 1833–1845. [[CrossRef](#)]
16. Ottesen, J.T.; Danielsen, M. Modeling ventricular contraction with heart rate changes. *J. Theor. Biol.* **2003**, *222*, 337–346. [[CrossRef](#)]
17. Gesenhues, J.; Hein, M.; Albin, T.; Rossaint, R.; Abel, D. Cardiac Modeling: Identification of Subject Specific Left-Ventricular Isovolumic Pressure Curves. *IFAC-PapersOnLine* **2015**, *48*, 581–586. [[CrossRef](#)]
18. Westerhof, N.; Elzinga, G.; Sipkema, P. An artificial arterial system for pumping hearts. *J. Appl. Physiol.* **1971**, *31*, 776–781. [[CrossRef](#)]
19. Burattini, R.; Knowlen, G.G.; Campbell, K.B. Two arterial effective reflecting sites may appear as one to the heart. *Circ. Res.* **1991**, *68*, 85–99. [[CrossRef](#)]
20. O'Rourke, M.F. Pressure and flow waves in systemic arteries and the anatomical design of the arterial system. *J. Appl. Physiol.* **1967**, *23*, 139–149. [[CrossRef](#)]
21. Wetterer, E.; Kenner, T. *Grundlagen der Dynamik des Arterienpulses*; Springer: Berlin/Heidelberg, Germany, 1968.
22. O'Rourke, M.F.; Avolio, A.P. Pulsatile flow and pressure in human systemic arteries. Studies in man and in a multibranch model of the human systemic arterial tree. *Circ. Res.* **1980**, *46*, 363–372. [[CrossRef](#)] [[PubMed](#)]
23. Stergiopoulos, N.; Young, D.F.; Rogge, T.R. Computer simulation of arterial flow with applications to arterial and aortic stenoses. *J. Biomech.* **1992**, *25*, 1477–1488. [[CrossRef](#)]
24. Westerhof, N.; Bosman, F.; De Vries, C.J.; Noordergraaf, A. Analog studies of the human systemic arterial tree. *J. Biomech.* **1969**, *2*, 121–143. [[CrossRef](#)]
25. Avolio, A.P. Multi-branched model of the human arterial system. *Med. Biol. Eng. Comput.* **1980**, *18*, 709–718. [[CrossRef](#)] [[PubMed](#)]
26. Lu, K.; Clark, J.W., Jr.; Ghorbel, F.H.; Ware, D.L.; Bidani, A. A human cardiopulmonary system model applied to the analysis of the Valsalva maneuver. *Am. J. Physiol. Heart Circ. Physiol.* **2001**, *281*, H2661–H2679. [[CrossRef](#)] [[PubMed](#)]
27. Gesenhues, J.; Hein, M.; Habigt, M.; Mechelinck, M.; Albin, T.; Abel, D. Nonlinear object-oriented modeling based optimal control of the heart: Performing precise preload manipulation maneuvers using a ventricular assist device. In Proceedings of the 2016 European Control Conference (ECC), Aalborg, Denmark, 29 June–1 July 2016; pp. 2108–2114.
28. National Research Council Committee for the Update of the Guide for the Care and Use of Laboratory Animals. The National Academies Collection: Reports Funded by National Institutes of Health. In *Guide for the Care and Use of Laboratory Animals*; National Academies Press, National Academy of Sciences: Washington, DC, USA, 2011.
29. Pierce, E. Wikipedia, File:Heart normal.svg. Available online: https://en.wikipedia.org/wiki/File:Heart_normal.svg (accessed on 16 March 2022).
30. Baan, J.; Van Der Velde, E.T.; De Bruin, H.G.; Smeenk, G.J.; Koops, J.; Van Dijk, A.D.; Temmerman, D.; Senden, J.; Buis, B. Continuous measurement of left ventricular volume in animals and humans by conductance catheter. *Circulation* **1984**, *70*, 812–823. [[CrossRef](#)]
31. De Vroomen, M.; Cardozo, R.H.L.; Steendijk, P.; van Bel, F.; Baan, J. Improved contractile performance of right ventricle in response to increased RV afterload in newborn lamb. *Am. J. Physiol. Heart Circ. Physiol.* **2000**, *278*, H100–H105. [[CrossRef](#)]
32. Steendijk, P.; Baan, J. Comparison of intravenous and pulmonary artery injections of hypertonic saline for the assessment of conductance catheter parallel conductance. *Cardiovasc. Res.* **2000**, *46*, 82–89. [[CrossRef](#)]
33. Liu, Z.; Brin, K.P.; Yin, F.C. Estimation of total arterial compliance: An improved method and evaluation of current methods. *Am. J. Physiol.* **1986**, *251 Pt 2*, H588–H600. [[CrossRef](#)]
34. Brimiouille, S.; Maggiorini, M.; Stephanazzi, J.; Vermeulen, F.; Lejeune, P.; Naeije, R. Effects of low flow on pulmonary vascular flow-pressure curves and pulmonary vascular impedance. *Cardiovasc. Res.* **1999**, *42*, 183–192. [[CrossRef](#)]
35. Chung, D.C.; Niranjani, S.C.; Clark, J.W., Jr.; Bidani, A.; Johnston, W.E.; Zwischenberger, J.B.; Traber, D.L. A dynamic model of ventricular interaction and pericardial influence. *Am. J. Physiol.* **1997**, *272 Pt 2*, H2942–H2962. [[PubMed](#)]
36. Hein, M.; Roehl, A.B.; Baumert, J.H.; Bleilevens, C.; Fischer, S.; Steendijk, P.; Rossaint, R. Xenon and isoflurane improved biventricular function during right ventricular ischemia and reperfusion. *Acta Anaesthesiol. Scand.* **2010**, *54*, 470–478. [[CrossRef](#)] [[PubMed](#)]
37. Gesenhues, J.; Hein, M.; Ketelhut, M.; Habigt, M.; Rüschen, D.; Mechelinck, M.; Albin, T.; Leonhardt, S.; Schmitz-Rode, T.; Rossaint, R.; et al. Benefits of object-oriented models and ModeliChart: Modern tools and methods for the interdisciplinary research on smart biomedical technology. *Biomed. Tech.* **2017**, *62*, 111–121. [[CrossRef](#)]
38. Segers, P.; Verdonck, P.; Deryck, Y.; Brimiouille, S.; Naeije, R.; Carlier, S.; Stergiopoulos, N. Pulse pressure method and the area method for the estimation of total arterial compliance in dogs: Sensitivity to wave reflection intensity. *Ann. Biomed. Eng.* **1999**, *27*, 480–485. [[CrossRef](#)] [[PubMed](#)]

39. Stergiopoulos, N.; Meister, J.J.; Westerhof, N. Simple and accurate way for estimating total and segmental arterial compliance: The pulse pressure method. *Ann. Biomed. Eng.* **1994**, *22*, 392–397. [[CrossRef](#)] [[PubMed](#)]
40. Gesenhues, J.; Hein, M.; Ketelhut, M.; Albin, T.; Abel, D. Towards Medical Cyber-Physical Systems: Modelica and FMI based Online Parameter Identification of the Cardiovascular System. In Proceedings of the 12th International Modelica Conference, Prague, Czech Republic, 15–17 May 2017; Linköping University Electronic Press: Linköping, Sweden, 2017; pp. 613–621.
41. Brimiouille, S.; Wauthy, P.; Ewalenko, P.; Rondelet, B.; Vermeulen, F.; Kerbaul, F.; Naeije, R. Single-beat estimation of right ventricular end-systolic pressure-volume relationship. *Am. J. Physiol. Heart Circ. Physiol.* **2003**, *284*, H1625–H1630. [[CrossRef](#)] [[PubMed](#)]
42. Freeman, G.L.; Little, W.C.; O'Rourke, R.A. The effect of vasoactive agents on the left ventricular end-systolic pressure-volume relation in closed-chest dogs. *Circulation* **1986**, *74*, 1107–1113. [[CrossRef](#)] [[PubMed](#)]
43. Little, W.C.; Cheng, C.P.; Mumma, M.; Igarashi, Y.; Vinten-Johansen, J.; Johnston, W.E. Comparison of measures of left ventricular contractile performance derived from pressure-volume loops in conscious dogs. *Circulation* **1989**, *80*, 1378–1387. [[CrossRef](#)] [[PubMed](#)]
44. Burkhoff, D.; Sugiura, S.; Yue, D.T.; Sagawa, K. Contractility-dependent curvilinearity of end-systolic pressure-volume relations. *Am. J. Physiol.* **1987**, *252*, H1218–H1227. [[CrossRef](#)]
45. Kass, D.A.; Beyar, R.; Lankford, E.; Heard, M.; Maughan, W.L.; Sagawa, K. Influence of contractile state on curvilinearity of in situ end-systolic pressure-volume relations. *Circulation* **1989**, *79*, 167–178. [[CrossRef](#)]
46. Nordhaug, D.; Steensrud, T.; Korvald, C.; Aghajani, E.; Myrmet, T. Preserved myocardial energetics in acute ischemic left ventricular failure—Studies in an experimental pig model. *Eur. J. Cardiothorac. Surg.* **2002**, *22*, 135–142. [[CrossRef](#)]
47. Vandenberghe, S.; Segers, P.; Steendijk, P.; Meyns, B.; Dion, R.A.; Antaki, J.F.; Verdonck, P. Modeling ventricular function during cardiac assist: Does time-varying elastance work? *ASAIO J.* **2006**, *52*, 4–8. [[CrossRef](#)] [[PubMed](#)]
48. Sack, K.L.; Dabiri, Y.; Franz, T.; Solomon, S.D.; Burkhoff, D.; Guccione, J.M. Investigating the Role of Interventricular Interdependence in Development of Right Heart Dysfunction During LVAD Support: A Patient-Specific Methods-Based Approach. *Front. Physiol.* **2018**, *9*, 520. [[CrossRef](#)] [[PubMed](#)]
49. Cingolani, H.E.; Perez, N.G.; Cingolani, O.H.; Ennis, I.L. The Anrep effect: 100 years later. *Am. J. Physiol. Heart Circ. Physiol.* **2013**, *304*, H175–H182. [[CrossRef](#)] [[PubMed](#)]
50. Westerhof, N.; Lankhaar, J.W.; Westerhof, B.E. The arterial Windkessel. *Med. Biol. Eng. Comput.* **2009**, *47*, 131–141. [[CrossRef](#)] [[PubMed](#)]